Damage and failure of triaxial braided composites under multi-axial stress states

Tobias Wehrkamp-Richter[a,*], Roland Hinterhölzl[a], Silvestre T. Pinho[b]

[a] *Institute for Carbon Composites, Technische Universität München, Faculty for Mechanical Engineering, Boltzmannstr. 15, D-85748 Garching b. München, Germany*
[b] *Department of Aeronautics, Imperial College London, SW7 2AZ London, United Kingdom*

Abstract

Damage and failure of triaxial braided composites under multi-axial stress states was investigated. In order to introduce different multi-axial stress states in the material, uni-axial tensile tests were performed at different off-axis orientations. Three braid architectures, comprising braiding angles of 30°, 45° and 60° were each loaded parallel to their axial, transverse and braid yarn direction. Digital image correlation measurement techniques were used to quantify the effects of the textile architecture and its heterogeneity on the strain field, to identify and locate constituent failure mechanisms and to investigate damage initiation and development. In order to identify the driving physical mechanisms behind the material non-linearity, the evolution of the damage variable and the accumulated inelastic strain was quantified using incremental loading/unloading experiments. A high-speed camera was employed in order to study the dynamic nature of catastrophic failure. The triaxial braids within this study exhibited severe non-linearities in the mechanical response before final failure as a result of extensive matrix cracking. While we found the underlying textile architecture to slightly reduce the elastic properties compared to equivalent tape laminates, it functions as a natural crack arresting grid. As a result of this mechanism, braids under certain load conditions were capable of withstanding a higher strain to failure, even if a large portion of the specimen surface was saturated with matrix cracks. The accompanying mechanical behaviour can be desirable in the design of crash absorbing or pseudo-ductile materials. An additional failure mode intrinsic to the textile architecture was encountered for loading in the heavily undulated braid yarn direction. Due to yarn straightening and out-of-plane movements, braided composites were found to fail as a result of large scale delaminations accompanied by progressive fibre bundle pull-out.

Keywords: A. Textile composites; B. Non-linear behaviour; Matrix cracking; E. Braiding

1. Introduction

Applying new lightweight materials, such as carbon fibre reinforced plastics (CFRP), allows a significant reduction in structural weight and carbon dioxide emissions. In these high-volume production industries, current manufacturing technologies face a twofold challenge: cost and cycle time. Braiding combines an automated and reproducible process together with an excellent

*Corresponding author: wehrkamp-richter@lcc.mw.tum.de; tel. +49 89 289 10433; fax. +49 89 289 15097

rate of material deposition for mass-production of high-performance structures. In braided composites, yarns of several thousand carbon fibres are intertwined and positioned on a mandrel to produce geometries with complex cross-sections. Two-dimensional (2D) triaxial braids comprise an integrated structure of yarns oriented in three in-plane directions, which makes them a well-suited choice for multi-axial loading. Their natural through-thickness reinforcement promises excellent specific energy absorption characteristics [1] in combination with higher delamination resistance compared to tape laminates [2, 3]. Mechanical in-plane properties, however, suffer from the textile nature of braids, as the intertwining yarns inevitably exhibit a certain degree of out-of-plane and in-plane waviness. Hence, a reduction of stiffness and strength can be observed compared to unidirectional composites. The inherent textile nature, which includes a multitude of curved yarn interfaces, resin rich areas and nesting of multiple plies, yields a complex damage and failure behaviour. In addition, the manufacturing process creates a heterogeneous fibre assembly which can cause significant variations of the material properties across a braided composite structure. As a result, investigations on multiple textile architectures are usually inevitable for the development of robust design allowables.

The determination of representative mechanical properties for braided composites remains a challenging task. Due to the complex textile architecture of braided composites, standard test methods developed for tape laminates may not be applicable. To address this issue, modified specimen dimensions for textile composites based on the ASTM D3039 standard [4] were proposed by [5].[6] conducted an experimental programme to characterise the mechanical response of triaxial braided composites. Using Moiré interferometry to obtain the displacement field on the specimen's surface and X-ray radiography, the damage development was investigated under longitudinal and transverse loading conditions. Multiple matrix cracks and delaminations were observed, in particular when loading occurred transverse to the axial yarns.[3] compared the performance of triaxial braid architectures to laminates manufactured from fabrics and prepreg tape. A considerable strength reduction in the longitudinal direction was observed, which was attributed to a combination of out-of-plane waviness as well as fibre damage in the yarns as a result of the braiding process.[7] investigated the effect of the resin system on damage development in braided composites using digital image correlation (DIC) techniques. A reduced onset and extent of damage was observed when applying a toughened instead of an untoughened epoxy system.[8] proposed a methodology to study damage initiation and development in different textile composites using a combination of full-field strain measurement obtained through DIC, acoustic emission (AE), X-ray computed tomography (CT) and microsections on flat coupons exposed to specific load levels.[9, 10] applied this approach to a 45° 1x1 triaxial braided composite and investigated damage mechanisms in different off-axis directions under tensile loading.

The present experimental study serves two major objectives. The first goal is to investigate the non-linear mechanical response of different triaxial braided carbon/epoxy composites under multi-axial stress states, which are achieved through off-axis tensile tests. For this purpose, straight-sided specimens of three braid architectures shown in Fig. 1, comprising a braiding angle θ of 30°, 45° and 60° are each tested in their axial (x), transverse (y) and braid fibre

direction (1F).

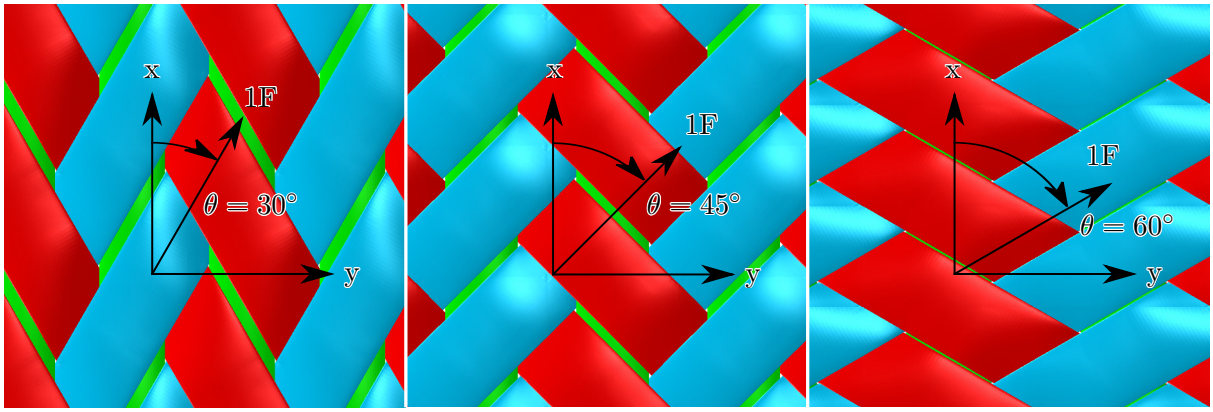


Figure 1: Triaxial braid architectures under investigation: [0/±30],[0/±45] and [0/±60]

An overview of the test cases and their corresponding stress state is displayed in Fig. 2. The configurations aim to represent the characteristic manufacturing variability encountered across a typical braided component [11]. After monotonically loading an initial test series up to final failure, a subsequent series employed incremental load cycles, which include loading, unloading and reloading. Following the approach described by [12], the evolution of macroscopic damage and inelastic strain is investigated, as it provides an insight into the physical mechanisms driving non-linearities within the material. Secondly, strong emphasis is put on the characterisation of the complex material damage and failure behaviour. DIC measurement techniques are used to quantify the effects of the textile architecture and its heterogeneity on the strain field, identify and locate constituent failure mechanisms and investigate damage initiation and development. Microsections of the specimen are analysed for the geometrical material characterisation and assessment of failure mechanisms in the thickness direction. A high-speed camera is employed in order to study the dynamic nature of catastrophic failure by identifying the consecutive short-term failure events. This information can serve as baseline for the development of a simulation model capable of predicting the constitutive behaviour of triaxial braided composites.

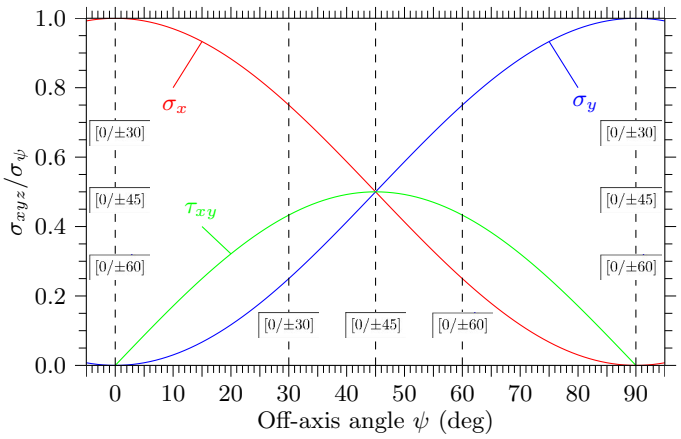


Figure 2: Test cases with the corresponding multi-axial stress states in principal coordinates (xyz) as a function of uni-axial loading σ_ψ at an off-axis angle ψ

2. Experiments

2.1. Material systems

The materials investigated in this study feature two-dimensional 2×2 triaxial braided preforms manufactured from Toho-Tenax HTS40 F13 12K (800 tex) untwisted yarns for both the axial and braid yarn direction in combination with a Hexcel HexFlow RTM 6 epoxy resin. All three braid architectures, with a nominal braiding angle of 30°, 45° and 60° were manufactured on a Herzog radial braiding machine with 176 bobbins. Single layers of triaxial braid were produced by over-braiding on a cylindrical mandrel which was guided through the braiding point by a robot at constant axial take-up speed as shown in Fig. 3. For each braiding angle, a different mandrel diameter was used in order to obtain a closed braid with full fibre coverage and hence avoid resin-rich areas. As a result, similar fibre areal weights were achieved. This allows a comparison of different braiding angles. Machine parameters were optimised such that the yarn dimensions of all braid architectures match as closely as possible. In order to produce flat panels, each braid layer was cut along the axial yarn direction, removed from the mandrel and subsequently flattened. Before cutting, a temperature-resistant tape was applied to all preform edges, such that fibre distortions during subsequent handling operations were minimised.

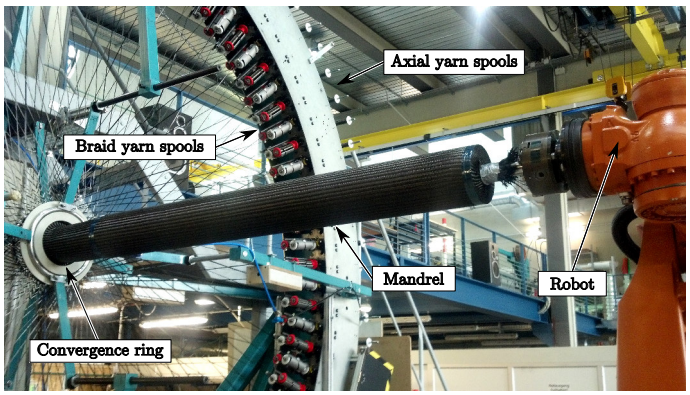


Figure 3: Overbraiding process

Composite plates were produced with a total of four triaxial braid plies each. The shift between unit cells (UC) in each ply was not controlled and can be considered to be random. For resin infusion, the Vacuum membrane Assisted Process (VAP) technology was selected to minimise void content and to yield similar fibre volume fractions (FVFs) in all plates as a result of constant compaction pressure. The resin system for all braid architectures consisted of a Hexcel HexFlow RTM 6 resin. This matrix material is a one-part untoughened 180° C cure epoxy system designed for the RTM process. After degassing, the resin was infused at 80° C and then cured at 180° C for 120 minutes. FVF measurements were obtained from three locations on each panel in accordance with ASTM D3171 [13]. The intra-yarn FVFs were determined by optical microscopy on polished cross-sections. For quality control and estimation of the textile architecture, each specimen was inspected with a photometric stereo sensor [14]. Based on fibre reflectance values from multiple images under different lighting conditions, the braiding angle distribution was measured over the entire specimen surface. In a subsequent step, the raw sensor pictures were processed with an image segmentation algorithm in order to extract features of the underlying meso-structure, such as yarn width and spacing. The averaged geometrical properties

are summarised in Table 1 together with the FVF measurements. Using an idealised model to render the measured geometrical data, the three braid architectures are visualised in Fig. 1.

Table 1: Properties of braid architectures under investigation

θ (deg)	Mandrel diameter (mm)	Thickness (mm)	Axial yarn spacing (mm)	Braid yarn spacing (mm)	Braid yarn width (mm)	FVF (%)	Axial yarn FVF (%)	Braid yarn FVF (%)	Axial yarn content (%)
29.95 ± 2.35	100	3.02 ± 0.04	3.63 ± 0.13	3.10 ± 0.57	2.91 ± 0.23	58.7 ± 0.9	66 ± 6	70 ± 5	29.1 ± 0.4
45.04 ± 2.09	120	2.99 ± 0.10	4.37 ± 0.38	3.05 ± 0.38	2.91 ± 0.21	55.9 ± 0.8	66 ± 4	70 ± 6	25.0 ± 0.3
57.47 ± 2.44	160	2.91 ± 0.09	5.30 ± 1.50	2.82 ± 0.23	2.85 ± 0.17	57.0 ± 0.2	63 ± 5	70 ± 5	19.3 ± 0.4

2.2. Test set-up

The selection of a test method to obtain representative material properties for braided composites is not straightforward.[7] and [15] highlighted differences in damage propagation for straight-sided and tubular specimens due to edge-initiated failure of a 60° triaxial braided composite subjected to transverse tension. A notched coupon geometry was proposed which yielded significantly larger strengths in relation to the standard tests. Contrarily, [10] found no significant influence of edge effects on the damage development for straight-sided specimens. The difference between cut and uncut coupon edges was investigated by [1] for biaxial braided composites. A substantial increase in strain to failure was observed for the case of uncut edges that preserve fibre continuity, together with a highly non-linear specimen dependent Poisson's effect and significant fibre reorientation. Within the presented study, we follow the methodology proposed by [8] and focus on straight-sided coupons based on ASTM D3039. In order to obtain a representative material response and minimise the effect of possible localised edge cracking, the specimen width must be large in relation to the size of the representative material unit cell. A width of 25 mm was selected in order to cover a minimum of two UCs, as proposed in [16]. For proper load introduction, glass fibre fabric tabs of 50 mm length were bonded to the specimen grip region, leaving a total gage length of 150 mm. In case the applied load direction was not aligned with one of the orthotropic axes, oblique tabs according to [17] were used to minimise stress concentrations due to the presence of material shear-extension coupling.

An electromechanical Hegewald & Peschke testing machine with hydraulic grips capable of loading 250 kN was operated at a constant head speed of 2 mm/min. All monotonic tests were performed under displacement control. The incremental loading tests were performed under load control, with the exception of the $[0/\pm 30]$ configuration under transverse tension due to a plateau-like stress-strain response. A maximum of seven loading, unloading and reloading cycles was selected in order to avoid the possibility of low-cycle fatigue phenomena [12]. Since [18] found viscous effects in biaxial carbon/epoxy braided composites to be of minor importance, each specimen was reloaded immediately after a preceding unloading cycle. The final loading cycle caused failure of the specimen. The maximum load levels of individual cycles were selected such that they specifically correspond to transition regions in the material response identified a priori in the monotonic tests. For all tests, full field measurement of surface strains was undertaken using the commercial DIC system GOM ARAMIS in 3D mode with a maximum camera resolution of 4 mega-pixels. A comprehensive description of DIC can be found in [19]. The field of view was centred at the coupon mid-section and covered approximately 70 mm of the gage length and the entire specimen width. A facet size of 17x17 pixels with a 2 pixels

overlap yielded a good compromise between measurement noise level and local field resolution. The linear strain in each facet was computed over a 3x3 subset window. In case not all adjacent facets exist, the strain in the centre facet was determined with a default validity quote of 55% [20]. Stress-strain curves were generated by averaging the full surface strain field, except for cases of significant surface cracking. Here, the macroscopic strain was calculated using a virtual extensometer over the complete measurement window to avoid any influence of artificial high strain computations in facets with underlying surface cracks. Final failure of the specimens was investigated with a PHOTRON SA5 high-speed camera operated at a rate of 20000 frames per second. For a field of view of similar size to the DIC, a maximum camera resolution of 384x880 pixels was achieved, with appropriate lighting provided by a 400 W flood light.

2.3. Experimental Methodology

For the monotonic tests, the elastic modulus was determined by a moving window least squares fit of the stress-strain curve. In the case of incremental loading, damage was characterised in terms of a macroscopic modulus degradation for each braided material. The corresponding scalar damage variable d was obtained after each unloading cycle according to [12]:

$$d_i = 1 - \frac{E_i}{E_0} \tag{1}$$

where E_i is the unloading modulus calculated from the end points of the loading and unloading part of cycle i as is shown in Fig. 4, such that the effects of a potential unloading/reloading hysteresis are minimised. The initial elastic modulus E_0 is calculated from a moving least squares fit in the first loading cycle. The accumulated inelastic strain component $\langle \varepsilon_{ie,i} \rangle$ was determined from the maximum nominal stress σ_i in cycle i by

$$\langle \varepsilon_{ie,i} \rangle = \langle \varepsilon_i \rangle - \frac{\sigma_i}{E_i}, \tag{2}$$

where $\langle \cdot \rangle$ denotes a volume averaged variable. The scalar damage variable and the inelastic residual strain represent homogenised material quantities caused by a combination of plasticity and failure modes occurring within the material, such as matrix cracking inside the yarns as well as in the resin pockets, intra- and inter-yarn delaminations, fibre-matrix debonding, and progressive fibre failure.

2.4. Analytical Modelling

The overall impact of the textile architecture on the elastic properties is approximated by comparing experimental data with equivalent tape laminates using classical lamination theory (CLT). Several modelling approaches exist for predicting the effect of waviness on the elastic properties of braided composites [21–23]. By comparing the experimental results to equivalent laminates without crimp, however, the possible knock-down of mechanical properties can be quantified directly. For triaxial braided composites, an equivalent laminate can be constructed by virtually separating the axial yarns, the braid yarns and the pure resin pockets. Each constituent is then modelled either with a single unidirectional ply in the respective fibre direction or represented by an isotropic layer, as is the case for the matrix pockets. The relative yarn ply

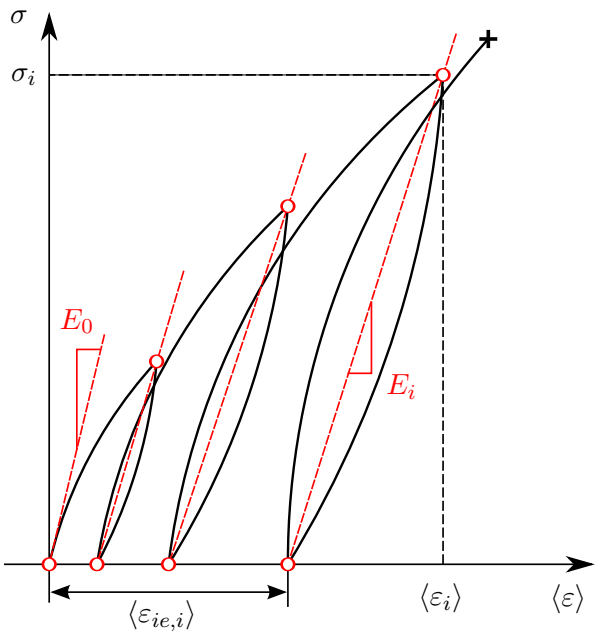


Figure 4: Determination of damage and inelastic strain from loading/unloading cycles

thicknesses in the laminate model correspond to the volume fractions of axial and braid yarn content given in Table 1. With the intra-yarn FVFs determined from microscopy, the relative thickness of the matrix ply is selected such that the overall FVF is satisfied. As a result of this approach, no textile architecture is considered, and a quantitative assessment of the mechanical property knock-down can be made in the linear-elastic regime. The homogenised elastic properties of the plies given in Table 3 were derived from the fibre and matrix properties given in Table 2 using the micromechanical equations from [24].

Table 2: Elastic properties for fibre and resin [25]

Fibre: Tenax HTS40 12k (800 tex)				Resin: RTM 6	
E_{1f} (MPa)	E_{2f} (MPa)	G_{12f} (MPa)	ν_{12f}	E_m (MPa)	ν_m
210000	18000	21800	0.305	2890	0.35

Table 3: Homogenised elastic properties of the unidirectional plies

Intra-yarn FVF (%)	E_1 (MPa)	E_2 (MPa)	G_{12} (MPa)	ν_{12}
63	133369	8660	4364	0.322
66	139583	9087	4705	0.320
70	147867	9709	5236	0.319

3. Results and Discussion

3.1. Elastic behaviour

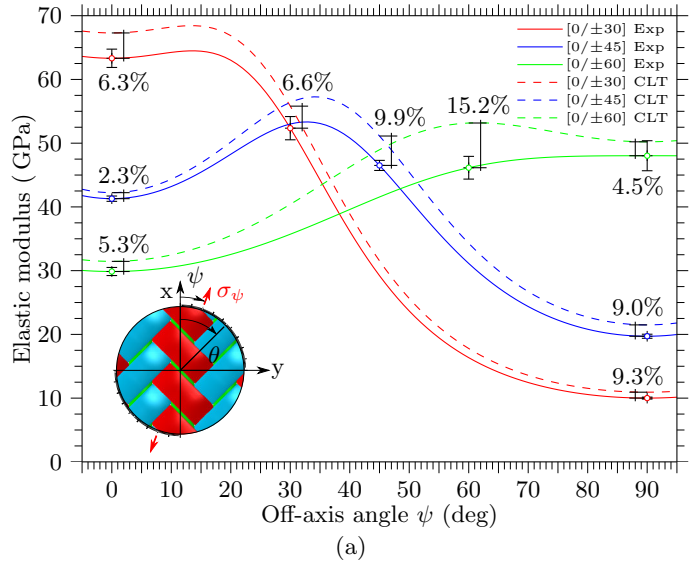
The linearised elastic moduli of the three braid architectures are compared to their respective CLT predictions in Fig. 5(a) as a function of the off-axis angle ψ. Assuming orthotropic material behaviour, the missing experimental in-plane shear modulus G_{xy} can be calculated from the off-axis Young's modulus in braid yarn direction (1F). This enables us to highlight differences between experiments and analytical predictions under arbitrary off-axis angles through a mere

transformation of the stiffness matrix. To compare the three braided configurations, the elastic moduli were normalised to a FVF of 56 %, and error bars indicate one standard deviation.

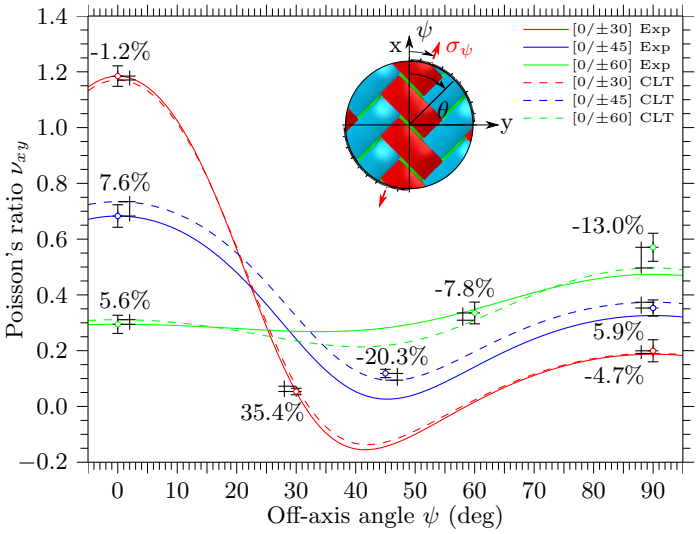
Due to CLT neglecting any undulation, it generally predicts larger moduli in relation to the experimental results. For loading in the x direction, only a minor decrease of the material properties can be observed. Here, the total homogenised stiffness is composed of a substantial contribution of the predominantly straight axial yarns superimposed by the load carrying capability of the undulated braid yarns. Most of the stiffness drop in this direction may be attributed to a combination of multiple textile phenomena: the presence of minor fibre in-plane and out-of-plane waviness in the axial yarns caused by the braiding process in combination with nesting and uneven compaction. Additionally, the axial fibre bundles tend to spread in regions where they are primarily surrounded by matrix pockets and lack support from adjacent braid yarns. Despite having the highest ratio of axial fibre volume content, the [0/±30] configuration exhibits the largest knock-down in x direction. This tendency is consistent with a higher contribution of the wavy braid yarns to the overall stiffness. As expected, this configuration yields the highest modulus in the x direction, which makes it a preferable choice for structures primarily subjected to bending loads.

The Young's moduli in the 1F direction are significantly lower compared to their equivalent laminate counterparts. This case yields the most severe reduction of the overall mechanical properties, as the heavily undulated braid yarns are loaded in their longitudinal direction. With increasing braiding angle, experimental and predicted moduli in 1F direction deviate progressively. The accompanying increase in braid yarn volume fraction combined with a larger bias orientation of the axial yarns contribute more and more to a degradation of the elastic properties, with a maximum relative error of 15.2 % for the [0/±60] braid. The stiffness reduction observed in the y direction is slightly larger than in the x direction. Here, no fibres are directly aligned with the load. In particular the axial yarns only contribute to the overall stiffness through their matrix-dominated transverse properties. Hence, any slight longitudinal contribution provided by the undulating braid yarns is amplified, even if the bias angle between the load direction and the braid fibre orientation is considerably high. A maximum relative error of 9.3 % can be observed for the [0/±30] case, in which the elastic modulus of 10 GPa is only slightly higher than the transverse properties of the yarns.

Fig. 5(b) summarises the results from the Poisson's ratio measurements. Given that only ν_{xy} serves as input for the homogenised stiffness matrix, the experimental results for other load directions diverge from those obtained by transformation. The [0/±30] architecture exhibits the largest Poisson's ratio in the x direction due to the severe discrepancy of longitudinal and transverse stiffness and is comparable to results obtained by [3]. Furthermore, its specific lay-up induces an auxetic behaviour close to an off-axis angle of 40°, with a negative Poisson's ratio of approximately −0.1. As the braiding angle increases, the mismatch between longitudinal and transverse stiffness becomes less pronounced, with a tendency towards balanced Poisson's ratios for the [0/±60] material. Except for the 1F direction, where the large relative error is connected to the Poisson's ratio converging to a value close to zero, the deviations between experiments and predictions are comparable to those of the elastic moduli. However, with the Poisson's effect



(a)



(b)

Figure 5: Comparison of experimental and predicted Young's moduli (a) and Poisson's ratios (b) as a function of the off-axis angle ψ

comprising a ratio of transverse and longitudinal strain, no direct contribution of fibre waviness can be extracted. As a general observation, the analytical model provides a simple and robust method for approximating the elastic in-plane properties of all braid configurations. While it is not capable of directly capturing any fibre waviness and generally over-predicts the mechanical properties, it represents a viable tool for the determination of stiffness properties within a preliminary design phase, where usually only limited data on the detailed textile architecture is available.

3.2. Non-linear behaviour and damage characterisation

The non-linear mechanical behaviour of triaxial braided composites is highly anisotropic. Depending on the external state of loading, a variation of the tangent modulus can be attributed to a combination of material and geometrical mechanisms. The application of DIC allows us to investigate strain concentrations and characteristic damage morphology in terms of crack initiation and propagation on the specimen surface, and to assess their impact on the homogenised stress-strain response. The results of this investigation are discussed in the following sections

for three different monotonic loading conditions.

3.2.1. Loading in the axial (x) direction

Typical stress-strain curves are presented in Fig. 6 for loading the three braid architectures in the axial (x) direction. In addition, the superimposed strain fields on the specimen surface are displayed for load levels of primary interest, such as transition regions in the stress-strain curve, the appearance of a first visible surface crack, and ultimately before final failure of the specimen. If not directly visible, surface crack locations are indicated by artificially high local strains due to the underlying displacement discontinuity which, for large crack openings, also causes automatic removal of the underlying facet. The grey dashed lines represent the elastic properties and allow us to emphasise the non-linearities in the stress-strain curves for progressive loading.

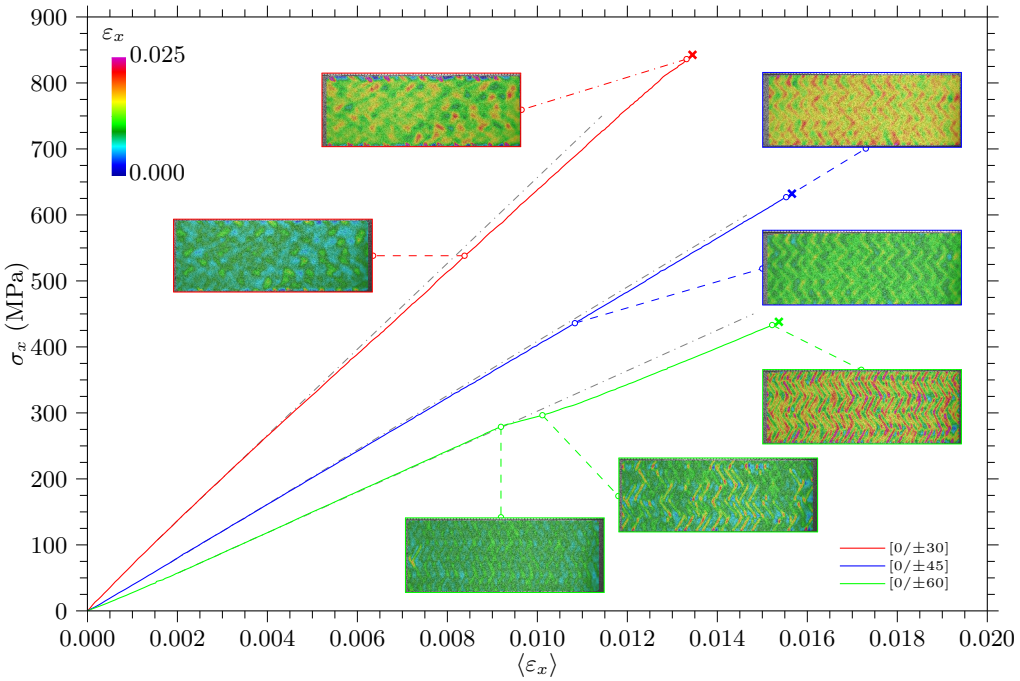


Figure 6: Representative stress-strain curves and local strain fields for loading in axial (x) direction

For the [0/±30] and the [0/±45] architecture, only a slight decrease in tangent modulus is observed. The surface strain fields for both configurations show strain concentrations at the resin-rich yarn-to-yarn junctions of the textile, but no evidence for matrix cracks except for localised edge damage shortly before final failure. As the overall mechanical response until final failure is dominated by the large stiffness contribution of the axial yarns loaded in the fibre direction, any possible geometrical and material non-linearity originating from the mesoscopic building blocks - the yarns and the matrix pockets - was found to have a negligible impact on the predominantly linear stress-strain response. Furthermore, while some of these phenomena are associated with a decrease in modulus, such as plasticity and damage, a competing stiffening effect on the stress-strain curve is induced by others. In the case of loading in the x direction, the primary load carrying carbon fibres in the axial yarns exhibit stiffening due to their non-Hookean constitutive behaviour [26–28]. At the same time, minor undulations in axial bundles caused by nesting effects of multiple braid plies diminish as the fibres align progressively with the load.

The braid bundles are subjected to a state of multi-axial stress, particularly in-plane shear in the case of a braiding angle of 45°. The resulting non-linear contribution, however, is small, also due to fact that it is simultaneously counteracted by a lateral fibre reorientation in load direction. The [0/±60] architecture exhibits almost linear behaviour up to a global threshold strain level of approximately 0.9 %. Up to this point, strain concentrations intensify at the yarn cross-over points until first matrix cracks nucleate at multiple locations on the specimen surface parallel to the braid fibre direction, as a result of their combined shear and transverse tensile loading. Within each braid yarn, they propagate along one fibre direction until they are arrested at the adjacent intersecting bundle. Subsequently, a crack appears in the other braid fibre direction - possibly promoted by the stress concentrations of the preceding crack tip - thus creating a zig-zag crack pattern across the specimen width. Unlike in a tape laminate, for example in a cross-ply laminate where matrix cracks may easily propagate across the entire coupon width, the textile architecture of braids acts as a crack stopper. Similar findings are also reported in [10]. Above the threshold strain, crack development can be directly correlated with a bulge in the stress-strain curve, accompanied by a sudden decrease in modulus. As the specimen is further loaded and saturating with cracks, the crack density increases from a single crack per yarn to an average of 2-3 cracks while the tangent modulus subsequently converges back to its initial magnitude. This stiffening effect may be the product of two overlying mechanisms: Firstly, after the braid yarns crack and become more compliant, more loads are redistributed back into the axial fibres. Secondly, the formation of multiple cracks removes constraints in the material, which promotes further alignment of fibres in the load direction. A post-mortem micrograph normal to the axial yarns in Fig. 7 highlights the through-thickness crack formation in the [0/±60] braid. In contrast to the undamaged axial bundles, a maximum density of three matrix cracks per yarn is evident in the braid direction, with some additional cracking inside the resin pockets. These findings are consistent with the DIC results. Depending on the stacking configuration, dry yarns of adjacent plies and equal orientation nest into each other during compaction and create a locally merging fibre bundle without a visible interface. Hence, crack growth from one ply to another is facilitated in the through-thickness direction. Coalescing cracks of non-aligned fibre direction are rarely observed, except for a single case in which a crack migrates into a thin resin pocket and further into an adjacent yarn. Generally, a very limited number of delaminations confined to small regions around crack tips were observed for loading in longitudinal direction.

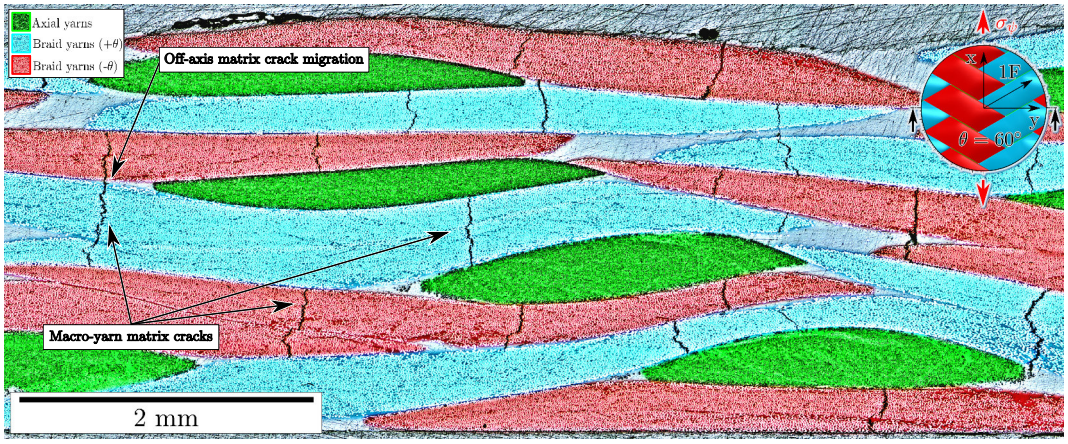


Figure 7: Crack pattern in a [0/±60] configuration subjected to axial loading obtained by optical microscopy

3.2.2. Loading in the transverse (y) direction

Severe non-linearities exist in all materials for loading in the transverse (y) direction as shown in Fig. 8. The [0/±45] and the [0/±60] braid exhibit a gradual decrease in stiffness. For the latter, no discrete cracks appear on the specimen surface, again with the exception of edge initiated damage. However, multiple sites of high strain concentrations at elevated load levels correlate with the positions of the underlying axial yarns, indicating subsurface failure events as a result of transverse tensile stresses. Considering the absence of any gaps between adjacent braid yarns, as can be seen in Fig. 1, their formation cannot be directly monitored, yet an investigation of the respective microsections confirmed their presence. A similar damage morphology was observed for the [0/±45] material. Initially, a gradual decrease in tangent modulus is attributed to the primary contribution of the braid fibre direction to the overall stress-strain curve through its non-linear shear behaviour. Unlike the previous case, the mechanical response is now not controlled by the large fibre stiffness in the load direction. Above a threshold stress of approximately 120 MPa, initial cracks appear in the axial yarns. Contrary to the [0/±60] braid, minor gaps in the textile allow local camera vision onto small segments of axial fibre bundles where most of the initial occurrences of cracks are identified. In the DIC image, a straight crack opens, running parallel to the axial fibre direction across the entire length of the visible uncovered section at the location of the gap between two braid yarns. Consecutively, both crack tips develop into the braid fibre direction at their opposing ends until they get arrested at the next cross-over point, again highlighting the step-wise crack development in braided composites. Supported by evidence from the micrographs in Fig. 9, the cracks in the axial yarns extend along their entire thickness. In case they contact an adjacent braid yarn, they further follow along the interface and create a localised delamination. After a certain length, a crack migration into this braid yarn can occur. Gradually, a complex crack network is created. This comprises several matrix cracks in neighbouring bundles connected by a multitude of delaminations or branching into the neat resin. As a consequence of this phenomenon, the stress-strain curve exhibits a significant degradation until final failure occurs when the tangent modulus approaches approximately a quarter of its initial magnitude.

The [0/±30] braid features the most complex damage behaviour for this load condition. Here, the material response can be separated into three distinct domains up to final failure: an approximately linear domain, a damage progression domain, and a saturation domain. As the applied load is increased in the linear domain, strain concentrations arise in the resin-rich areas between adjacent yarns, thus exposing the underlying textile architecture. When a critical load level is reached, the first matrix cracks form at the boundaries of adjacent yarns at a specific location across the specimen length. Their initial appearance can be correlated with the first major load drop, which marks the point of damage initiation at the end of the linear domain. While the damage morphology follows a similar pattern to the previous [0/±45] case, the effect on the stress-strain curve is considerably larger. In light of the fact that the [0/±30] material features the largest bias angle with respect to the fibres and the load direction, the compliance introduced by the formation of each crack can be correlated with small load drops. As the strain is further increased, the loads are redistributed and the stress level exhibits a stable plateau as

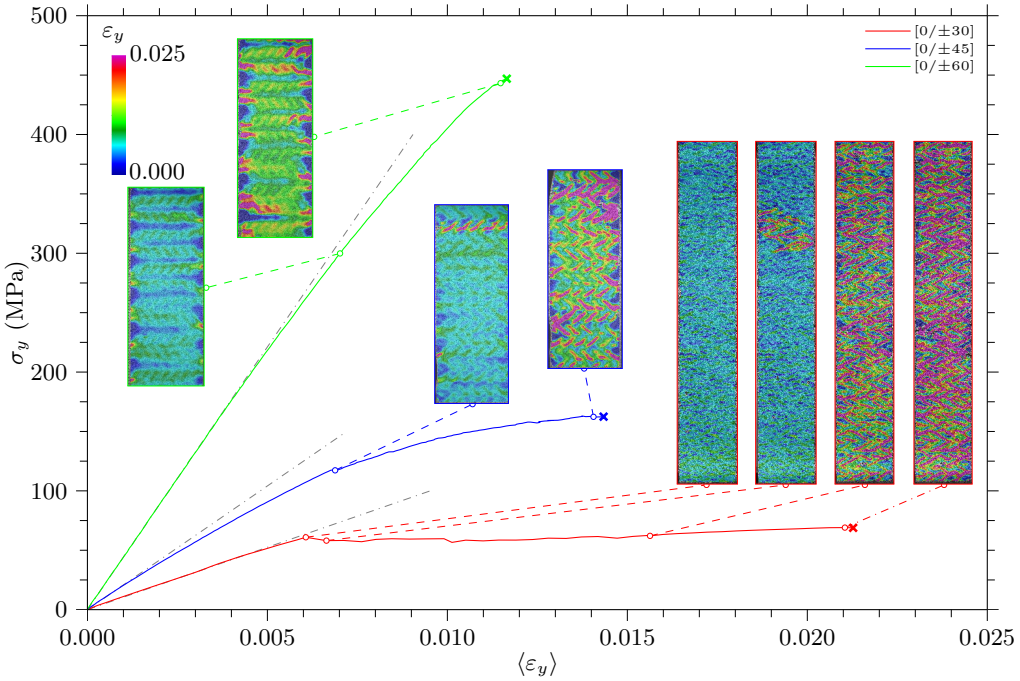


Figure 8: Representative stress-strain curves and local strain fields for loading in transverse (y) direction

a result of progressive damage development. This behaviour is associated with the continuing development of matrix cracks, originating from the initiation location on the coupon. When the entire specimen is saturated with cracks, a small increase in load can be observed. In this domain, the existing cracks exhibit further opening. Final failure of the specimen is induced when multiple cracks coalesce across the specimen width.

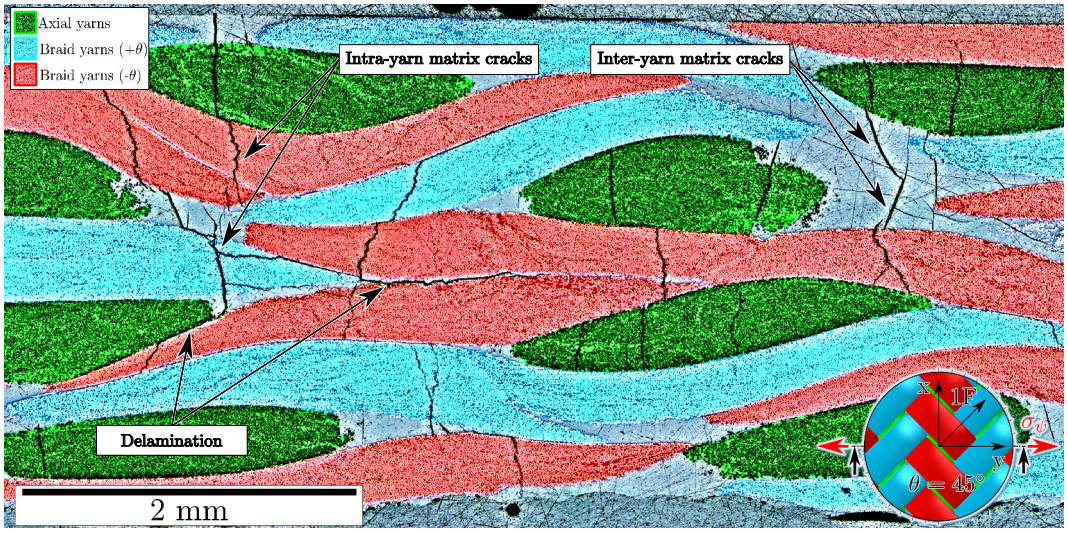


Figure 9: Crack pattern in a [0/±45] configuration subjected to transverse loading obtained by optical microscopy

3.2.3. Loading in braid yarn (1F) direction

The textile architecture has the greatest effect on the mechanical response for loading in the braid fibre direction ($1F$), as is shown in Fig. 10. Up to a homogenised strain level of $\langle\varepsilon_{1F}\rangle \approx 0.6\%$, all braid architectures exhibit approximately linear stress-strain behaviour.

Beyond this threshold point, distinct load drops can be attributed to a progressive failure mechanism intrinsic to the textile architecture: as the highly crimped braid yarns are aligned with the external load, they straighten along their longitudinal direction. Hence, intersecting

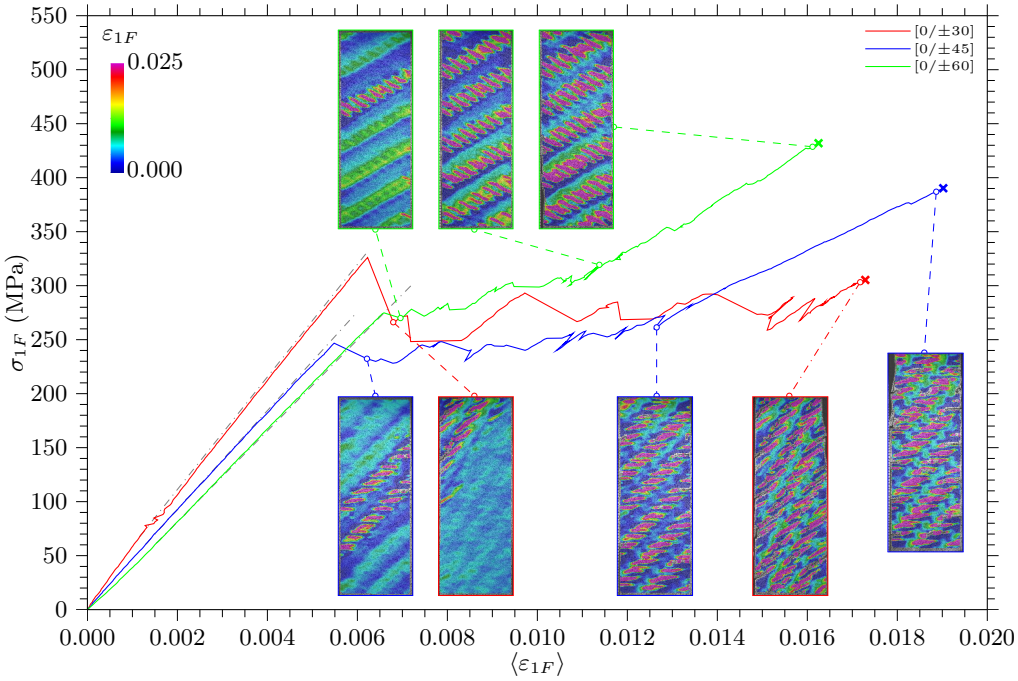


Figure 10: Representative stress-strain curves and local strain fields for loading in braid yarn (1F) direction

axial fibre bundles are subjected to an out-of-plane displacement which is at first inhibited by the overlying braid yarns and the support of adjacent plies in the through-thickness direction. Once the resulting out-of-plane stresses trigger failure in the interface, a large delamination zone is created and extends across the entire specimen width along a single subsurface axial yarn. Simultaneously, the localised loss of through-thickness support causes an abrupt pull-out of this fibre bundle, accompanied by several secondary matrix cracks in the overlying braid yarns. The DIC images in Fig. 10 detail the strain field after an initial pull-out event for each braid configuration. Due to the abrupt and unstable nature of this failure mode, a sudden increase in the homogenised strain combined with a slight load drop can be observed. When the applied strain is further increased, the progressive pull-out of fibre bundles fabricates a plateau-like stress-strain response. This behaviour shows similarities to the previously mentioned [0/±30] transverse load case, but originates from a different failure mechanism and at considerably higher stress.

Fig. 11 displays a detailed view of the strain field for the [0/±45] material after several axial yarns have debonded. The secondary matrix cracks are clearly visible and the heterogeneous shading on the coupon surface underlines the mismatch of out-of-plane displacement of adjacent axial yarns. When a nominal textile geometry derived from Table 1 is mapped onto the specimen surface, the locations of matrix cracks reveal that the pull-out effect is confined to every second axial bundle. If we consider the cross-sectional cut A-A, it becomes evident that the braid yarns oriented along the coupon width provide only limited resistance against out-of-plane deformations at the coupon surface. Without the through-thickness support of an adjacent layer, the outer plies tend to promote the initial formation of delamination and subsequent bundle pull-out in regions where the out-of-plane deformation is oriented to the outside of the specimen. While the first event was observed at a random location, probably triggered by the weakest unit cell, subsequent pull-outs progressively occur in direct proximity at the next but one bundle

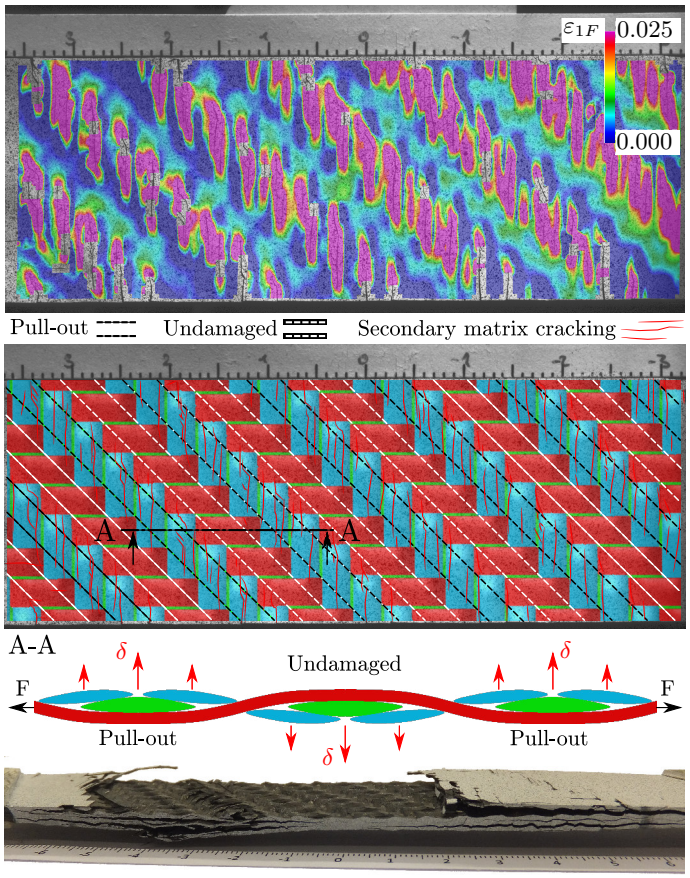


Figure 11: DIC surface strain field, crack pattern, failure mechanism and ply separation during ultimate failure of a [0/±45] braid subjected to loading in braid yarn (1F) direction

and propagate along the specimen gage length in both directions until a saturation stage is reached. The cascading nature of this failure mechanism indicates some weakening influence of braid yarns with multiple secondary matrix cracks. As a result of the textile architecture, these yarns are oriented along the specimen width, with some of them again inhibiting pull-out of the next potential axial bundle after one undulation interval. At the end of the plateau strain, the delaminations have completely interconnected in each of the three ply interfaces. After a full separation of the braided layers along the entire gage length, each of them acts as a separate entity, and the mechanical response is again governed by the braid fibres aligned with the load. For the [0/±45] and the [0/±60] architecture, the sustainable load can be approximately doubled compared to the plateau initiation before final failure. In addition to the many advantages of applying DIC measurement techniques to textile composites summarized in [9], the 3D DIC set-up allowed us to identify and measure the out-of-plane deformation of the braid bundles during the progressive pull-out mechanism.

3.3. Evolution of damage and inelastic strain

In order to identify the driving physical mechanisms behind the material non-linearity, the evolution of the homogenised damage variable and the accumulated inelastic strain is quantified as a function of the total strain in Fig. 13(a) and (b), respectively. Each of the data points corresponds to a completed cycle and a polynomial fit illustrates the average evolution of both variables up to the failure strain of the corresponding test series. Due to a problem in the data acquisition during the incremental loading/unloading tests parallel to the braid fibre direction

of the [0/±30]material, this test case is not included. The stress-strain response and strength of all loading/unloading tests were very similar to their monotonic counterparts, indicating that unloading and reloading had no substantial effect on the constituent failure mechanisms, as is highlighted in Fig. 12. Depending on the degree of damage, the unloading and reloading cycles
390 reveal hysteresis loops, possibly due to frictional effects at crack interfaces and failed fibre/matrix interfaces [1].

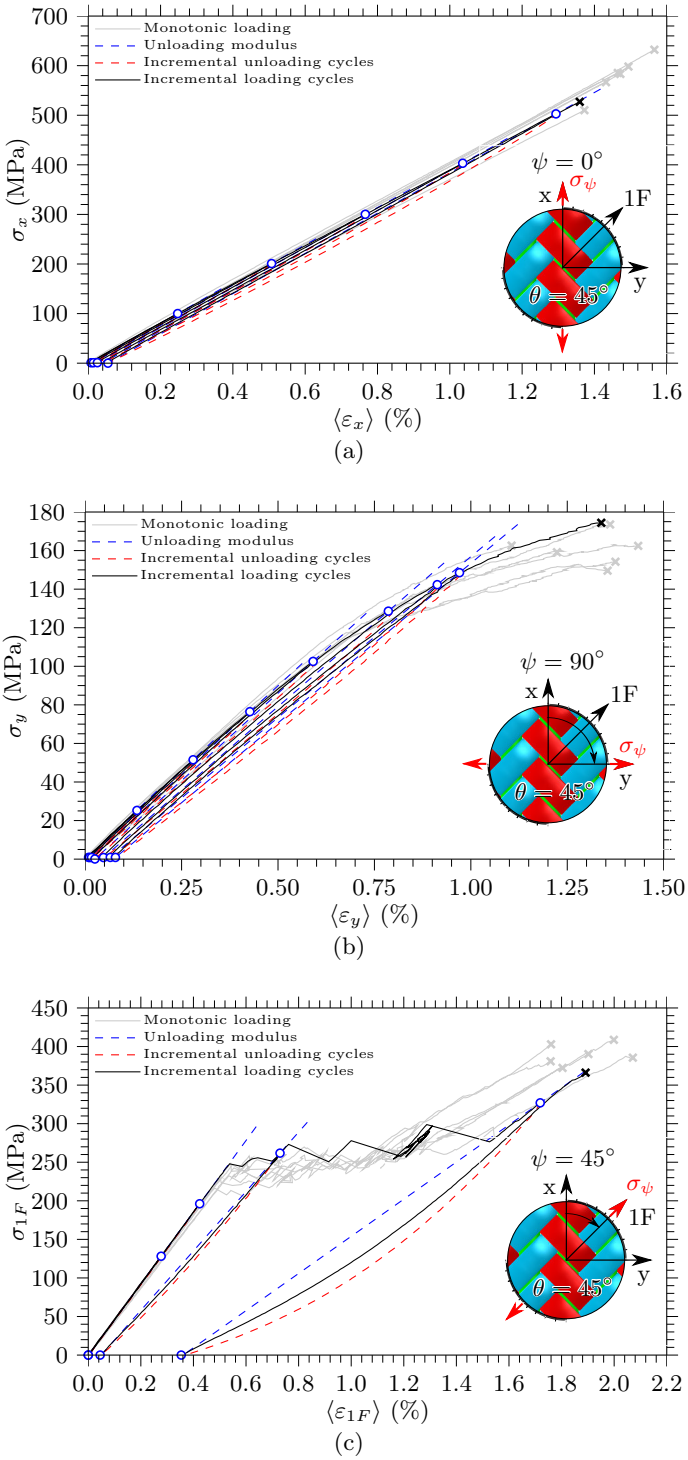


Figure 12: Comparison of monotonic and representative incremental loading/unloading stress-strain curves for the [0/±45] architecture loaded in the (a) axial, (b) transverse, (c) braid fibre direction

Consistently with the monotonic tests, only minor non-linearities are present in the material for cases in which the load is aligned with the axial fibre direction (x). Independently of the

braiding angle, the damage variable for the [0/±30] and the [0/±45] braided composite remains at a steady level below 5 %. The inelastic strain shows a gradual increase. However, with a maximum magnitude of 0.05 % at an average failure strain of about 1.3 %, the total contribution for all braid configurations in axial direction remains negligible. The [0/±60] configuration exhibits a negative damage variable which indicates a slight stiffening effect upon loading from a combination of initial axial yarn straightening. After the degradation at the onset of matrix cracking inside the braid yarns, the superimposed stiffening due to load redistribution and lateral fibre reorientation translates into a slight increase in both the damage variable and the accumulated inelastic strain until final failure. Recalling the stress-strain curves from Fig. 8, significant non-linearities occur for loading in the transverse direction. For both the [0/±60] and the [0/±45] cases, the damage variable and the inelastic strain grow steadily as a function of the applied strain. An accompanying increase of the damage variable at low strains suggests the presence of microscopic damage events. When the first macroscopic cracks appear in the axial and braid yarns at an applied strain of approximately 0.6 %, the rate of growth of the damage variable and the inelastic strain are amplified. Two separate domains in the mechanical response of the [0/±30] are clearly visible in the loading/unloading experiments. In the first domain, the highest gradual increase in damage amongst all architectures is accompanied by a negligible increase in inelastic strain. Here, strain concentrations arise at the yarn interfaces, but no macroscopic cracks are visible on the specimen surface yet. Following their first appearance at the initiation site and the subsequent propagation across the entire coupon, the increasing crack density can be correlated with an abrupt increase in both the damage variable and the inelastic strain. As the applied strain is further increased, and the coupon is saturating with cracks, the rate of damage and inelastic strain growth recedes consistently. Now, crack growth is replacing the formation of new cracks as the driving damage mechanism. Before final failure of the specimen, the modulus has degraded to almost 50 % of its initial value, at a considerable inelastic strain of 0.35 %.

Subdividing the mechanical response into two separate domains is also viable in the case of loading in braid fibre direction (1F). Before the first pull-out event, all materials follow an almost identical path, including negligible damage and inelastic strain accumulation. As soon as the first delamination zone forms and induces axial yarn pull-out, both the damage variable and the inelastic strain increase drastically. The transition into this failure mode is triggered at a slightly lower strain of 0.5 % for the [0/±45] case in comparison to the the [0/±60] configuration. During the progressive ply separation in both materials, the evolution of the damage variable again follows a very similar path. Due to its higher failure strain of more than 1.7 % and its earlier failure mode transition, the [0/±45] case is capable of sustaining a comparably larger loss in modulus and accumulation of inelastic strain before final failure than the [0/±30] braid subjected to transverse loading. If we consider that the increase in inelastic strain is negligible before the initial appearance of cracks in the [0/±45] transverse load case, where both braid yarn directions are predominantly loaded in shear and contribute significantly to the overall stiffness, we can conclude that the overall impact of plasticity in the yarns is small compared to the effects of matrix cracking. Having identified matrix cracking and delaminations as the

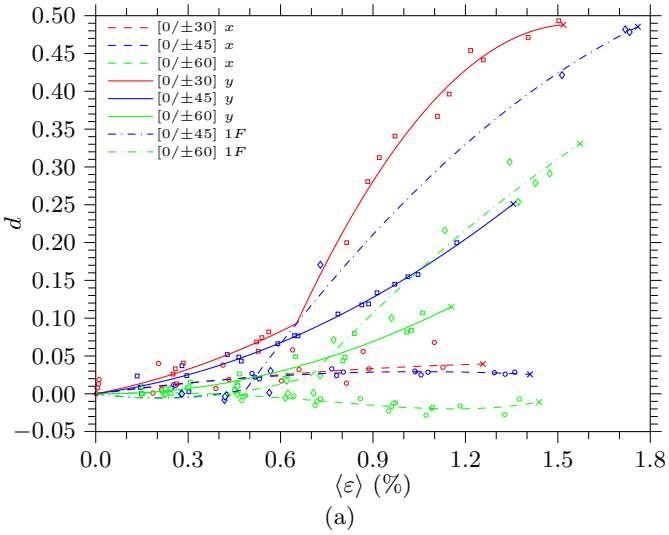


Figure 13: Evolution of the scalar damage variable d (a) and the accumulated inelastic strain $\langle \varepsilon_{ie} \rangle$ (b) as a function of applied strain

primary source of non-linearities in triaxial braids, we observe that both of these failure modes introduce significant damage and inelastic strain into the material.

3.4. Final failure modes

After investigating the non-linear mechanical behaviour, a better understanding of the mechanisms which trigger catastrophic failure is key to the design of more damage-tolerant braided composite materials. In Fig. 14, the development of final failure for a representative specimen of each test case is studied using a sequence of three images recorded with a high-speed camera. The first one highlights the state of the specimen immediately before failure with a maximum resolution of 0.05 ms. The second image captures the short-term formation of a fracture zone propagating across the entire coupon width. This process allows for very rapid movement of the fracture surfaces and is typically accompanied by a certain degree of motion blur. Lastly, the third image represents the post-mortem state. Since no data was available for the [0/±30] y configuration, we focus solely on the post-mortem inspection in this case.

All braid architectures loaded in take-up direction develop a bidirectional V-shaped fracture zone which extends across the coupon width along both intersecting braid fibre directions. The

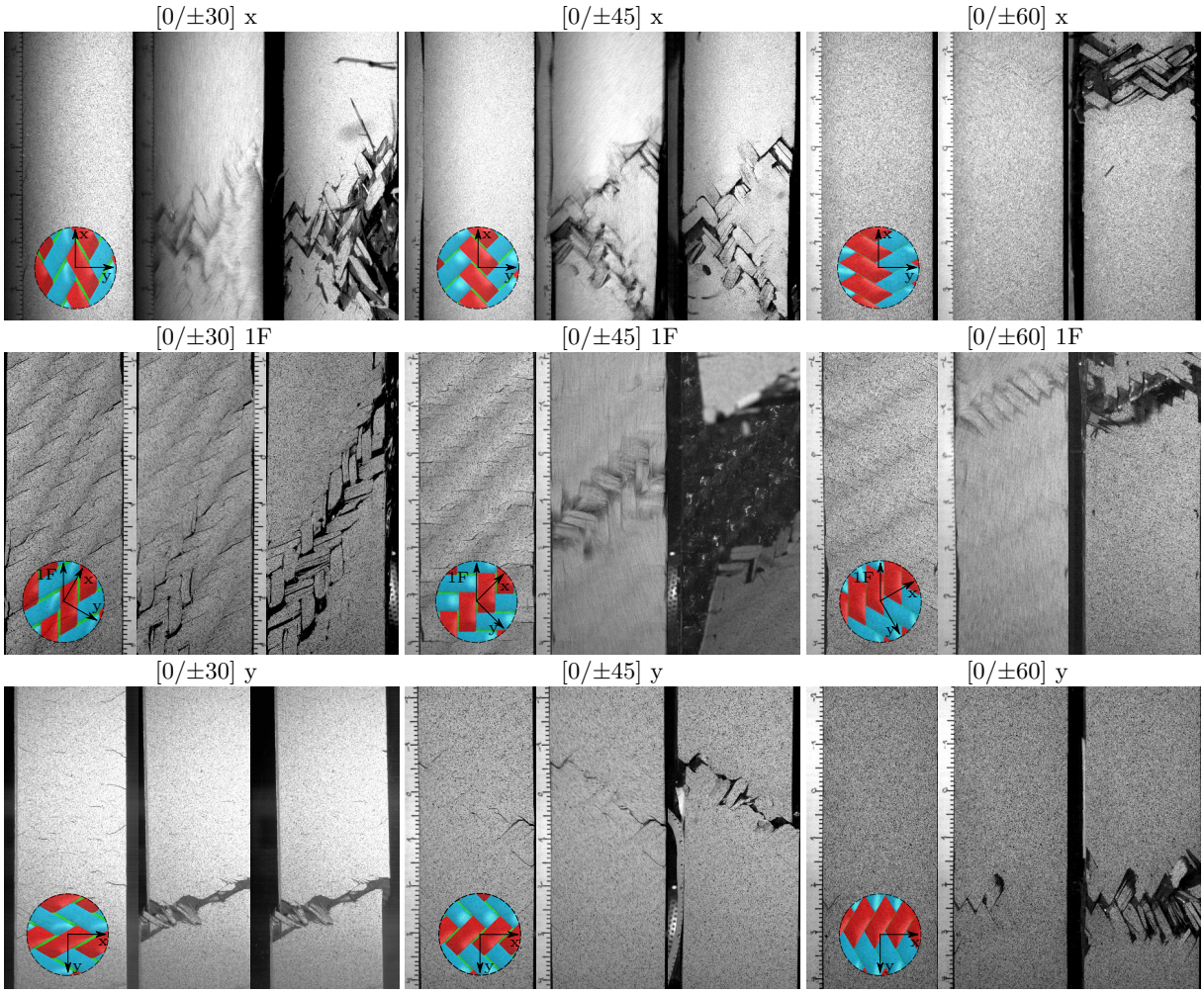


Figure 14: Final failure process recorded with a high-speed camera

absence of visible surface cracks and the initial axial movement of the specimen suggests that catastrophic failure for a braiding angle of 30° and 45° is triggered by rupture of axial yarns. Due to the resulting high amount of energy getting released, several additional fibre bundles disintegrate and large pieces of debris are explosively separated from the specimen. For the [0/±60] case, several matrix cracks propagate rapidly in a zig-zag pattern across the coupon immediately before catastrophic failure and further promote failure of the underlying axial yarns at the same location. Final failure of all materials loaded in 1F direction is dominated by fibre fracture in the load aligned braid yarns. After all plies have completely delaminated and the load is further increased, fibre bundles break at their respective yarn cross-over point. When viewed from the top, each yarn ruptures at an angle coincident with the intersecting braid fibre direction. With the ply losing its primary load carrying capability, a stair-case shaped band of cracked braid yarns propagates rapidly across the coupon width. Due to the excessive recoil, large pieces of individual layers may disintegrate and allow camera vision the fractured braid ply interface.In contrast to the previous cases, the final failure for the transverse load cases is confined to a small region. Here, a single macroscopic crack develops along one of the braid fibre directions, promoted by the previously existing matrix cracks. The intersecting braid yarns initially prevent a complete coupon separation. However, due to the opposing lateral movements of the fracture surfaces, they fail as a result of excessive rotation.

4. Conclusion

Within this study, the damage and failure behaviour of triaxial braided composites was investigated under multi-axial stress states introduced through uni-axial off-axis tests. Digital image correlation measurement techniques were used to quantify the effects of the textile architecture and its heterogeneity on the strain field, to identify and locate constituent failure mechanisms and to investigate damage initiation and development. Microsections of the specimen were analysed for the purpose of geometrical material characterisation and assessment of failure mechanisms in the thickness direction. The evolution of the damage variable and the accumulated inelastic strain was quantified using incremental loading/unloading experiments. A high-speed camera was employed in order to study the dynamic nature of catastrophic failure. The triaxial braids within this study exhibited severe non-linearities in the mechanical response before final failure. This phenomenon was primarily attributed to a complex damage behaviour composed of two characteristic mechanisms. In the first one, matrix cracks developed progressively in the yarns that were not aligned with the load direction. While we found the underlying textile architecture to slightly reduce the elastic properties compared to equivalent tape laminates, we conclude that it functions as a natural crack arresting grid and restricts the propagation of cracks to in between adjacent intersecting yarns, thus reducing their criticality. Loads can be redistributed without catastrophic failure of the material. In addition, a possible crack deflection can cause additional energy absorption. As a result of this mechanism, braids under certain load conditions were capable of withstanding a high strain to failure, even if a large portion of the specimen surface was saturated with matrix cracks. The accompanying mechanical behaviour can be desirable in the design of crash absorbing or pseudo-ductile materials. An additional failure mode intrinsic to the textile architecture was encountered for loading in the heavily undulated braid yarn direction. Due to yarn straightening induced out-of-plane deformations, braided composites were found to fail as a result of large scale delaminations accompanied by progressive fibre bundle pull-out. This information can further serve as a baseline for the development of a numerical model for predicting the non-linear constitutive behaviour of braided composites. Having identified the failure morphology to be severely affected by the underlying textile architecture, the necessity of a meso-scale modelling approach becomes evident. In addition to a realistic representation of the internal geometry after compaction of multiple braided layers, the potential development of a bundle pull-out mode requires failure to not only be captured inside the yarns or matrix pockets, but also at their respective interfaces.

Acknowledgements

The first author acknowledges the kind support of Dr. Markus Sause at the University of Augsburg. The authors also thank Dr. David Schultheiss for braiding and Monika Humbs for her assistance during manufacturing and mechanical testing.

References

[1] Pickett A, Fouinneteau M. Material characterisation and calibration of a meso-mechanical damage model for braid reinforced composites. Composites Part A: Applied Science and Manufacturing 2006;37(2):368 –77. CompTest 2004.

[2] Falzon PJ, Herszberg I, Bannister MK, Leong K, et al. Compression and compression-after-impact properties of 2-d braided carbon/epoxy composites. In: Proceedings of the First Australasian Congress on Applied Mechanics: ACAM-96. Institution of Engineers, Australia; 1996, p. 297.

[3] Falzon PJ, Herszberg I. Mechanical performance of 2-D braided carbon/epoxy composites. Composites Science and Technology 1998;58(2):253 –65.

[4] ASTM International . ASTM D3039 - Standard Test Method for Tensile Properties of Polymer Matrix Composite Materials. 2008.

[5] Masters JE, Portanova MA. Standard test methods for textile composites. NASA Contractor Report 4751; NASA; 1996.

[6] Masters JE, Ifju PG. A phenomenological study of triaxially braided textile composites loaded in tension. Composites Science and Technology 1996;56(3):347 –58.

[7] Littell JD, Binienda WK, Roberts GD, Goldberg RK. Characterization of damage in triaxial braided composites under tensile loading. Journal of Aerospace Engineering 2009;22(3):270 –9.

[8] Lomov S, Ivanov D, Truong T, Verpoest I, Baudry F, Vanden Bosche K, et al. Experimental methodology of study of damage initiation and development in textile composites in uniaxial tensile test. Composites Science and Technology 2008;68(12):2340 –9.

[9] Ivanov D, Ivanov S, Lomov S, Verpoest I. Strain mapping analysis of textile composites. Optics and Lasers in Engineering 2009;47(3-4):360 –70.

[10] Ivanov DS, Baudry F, Van Den Broucke B, Lomov SV, Xie H, Verpoest I. Failure analysis of triaxial braided composite. Composites Science and Technology 2009;69(9):1372 –80.

[11] Hans T, Cichosz J, Brand M, Hinterhlzl R. Finite element simulation of the braiding process for arbitrary mandrel shapes. Composites Part A: Applied Science and Manufacturing 2015;77:124 –32.

[12] Ladeveze P, LeDantec E. Damage modelling of the elementary ply for laminated composites. Composites Science and Technology 1992;43(3):257 –67.

[13] ASTM International . ASTM D3171 - Standard Test Methods for Constituent Content of Composite Materials. 2009.

[14] Thumfart S, Palfinger W, Eitzinger C. Accurate fibre orientation measurement for carbon fibre surfaces. Lecture Notes in Computer Science 2013;:75 – 82.

[15] Kohlman LW, Bail JL, Roberts GD, Salem JA, Martin RE, Binienda WK. A notched coupon approach for tensile testing of braided composites. Composites Part A: Applied Science and Manufacturing 2012;43(10):1680 –8.

[16] Minguet PJ, Fedro MJ, Gunther CK. Test methods for textile composites. NASA Contractor Report 4609; NASA; 1994.

[17] Sun C, Chung I. An oblique end-tab design for testing off-axis composite specimens. Composites 1993;24(8):619 –23.

[18] Kelkar AD, Whitcomb JD. Characterization and structural behavior of braided composites. Tech. Rep. DOT/FAA/AR-08/52; U.S. Department of Transportation, Federal Aviation Administration; 2009.

[19] Pan B, Qian K, Xie H, Asundi A. Two-dimensional digital image correlation for in-plane displacement and strain measurement: a review. Meas Sci Technol 2009;20(6).

[20] GOM Aramis User Manual; 6.1 ed. GOM mbH, D-38106 Braunschweig; 2009.

[21] Byun JH. The analytical characterization of 2-d braided textile composites. Composites Science and Technology 2000;60(5):705 –16.

[22] Potluri P, Manan A, Francke M, Day R. Flexural and torsional behaviour of biaxial and triaxial braided composite structures. Composite Structures 2006;75(1-4):377 –86.

[23] Potluri P, Manan A. Mechanics of non-orthogonally interlaced textile composites. Composites Part A: Applied Science and Manufacturing 2007;38(4):1216 –26.

[24] Chamis CC. Simplified composite micromechanics equations for strength, fracture toughness, impact resistance and environmental effects. Tech. Rep.; NASA Technical Memorandum 83696; 1984.

[25] Cichosz J, Wehrkamp-Richter T, Koerber H, Hinterhp̈lzl R, Camanho PP. Failure and damage characterization of (30) biaxial braided composites under multiaxial stress states. Composites Part A: Applied Science and Manufacturing 2016;90:748–59.

[26] Van Dreumel WH, Kamp JL. Non hookean behaviour in the fibre direction of carbon-fibre composites and the influence of fibre waviness on the tensile properties. Journal of Composite Materials 1977;11(4):461 –9.

[27] Djordjevic IM, Sekulic DR, Mitric MN, Stevanovic MM. Non-hookean elastic behavior and crystallite orientation in carbon fibers. Journal of Composite Materials 2010;44(14):1717 –27.

[28] Mandel U, Taubert R, Hinterhlzl R. Three-dimensional nonlinear constitutive model for composites. Composite Structures 2016;142:78 – 86.